Supplementary Materials for

Optimization of oxygen evolution activity by tuning e_g* band broadening in nickel oxyhydroxide

Haoyin Zhong, Xiaopeng Wang[*], Guangxin Sun, Yaxin Tang, Shengdong Tan, Qian He, Jun Zhang, Ting Xiong, Caozheng Diao, Zhigen Yu[*], Shibo Xi[*], Wee Siang Vincent Lee[*], Junmin Xue[*]

*Corresponding author. Email: msexuejm@nus.edu.sg (Junmin Xue); xi_shibo@isce2.a-star.edu.sg (Shibo Xi); msewxia@nus.edu.sg (Xiaopeng Wang); mseleew@nus.edu.sg (Wee Siang Vincent Lee); yuzg@ihpc.a-star.edu.sg (Zhigen Yu)

This PDF file includes:

Materials and Methods
Figs. S1 to S34
Tables S1-2
References 1-3

Materials and Methods

Materials. $Ni(NO)_3 \cdot 6H_2O$, $Fe(NO_3)_3 \cdot 9H_2O$, Urea, Sulfur, Selenium, Sodium phosphate monobasic, Potassium sulfate, Sodium selenite, and 5wt.% Nafion solution were purchased from the Sigma-Aldrich. These chemicals were reagent grade and used without further purification.

Synthesis of the X-Ni(OH)$_2$ (X=NiS$_2$, NiSe$_2$, Ni$_5$P$_4$)

(1) Synthesis of Ni(OH)$_2$ on carbon cloth. The $Ni(OH)_2$ was grown on the carbon cloth via a facile hydrothermal method. Before that, the carbon cloth was pre-treated under 500 °C for 1h in the air condition and dealt with Ultra-Violet Ozone for 30 min to make it fully hydrophilic. Next, 2mmol $Ni(NO)_3 \cdot 6H_2O$, 10mmol Urea were added into 35 mL DI water and stirred for 15 min to form uniform solution. One piece of carbon cloth with size of 2 cm × 3 cm was immersed into the solution. Then, they were transferred into a 50 mL Teflon-lined stainless-steel autoclave and kept at 120 °C for 10h. The obtained $Ni(OH)_2$ was then washed by DI water for three times to remove the solution and loosely adhered $Ni(OH)_2$ powder. Finally, the $Ni(OH)_2$ was dried under 70 °C in air for 4h.

(2) Preparation of NiS$_2$, NiSe$_2$, Ni$_5$P$_4$. When preparing NiS_2, the 2 cm × 3 cm carbon cloth loaded $Ni(OH)_2$ sample was placed at the downstream position in the crucible, while 400 mg sulfur powder was placed at the upstream position. The sample was kept at 400 °C for 2h under N_2 atmosphere and then cool down to temperature. After that, the obtained NiS_2 was washed using DI water and dried at 70 °C for 1h. The synthesis procedures of $NiSe_2$ and Ni_5P_4 were the same as that of NiS_2, except that the anion source was selenium and NaH_2PO_4 powder, respectively.

(3) Electrochemical-oxidation of NiS$_2$, NiSe$_2$, and Ni$_5$P$_4$ in 1 M KOH. The electro-oxidation process was conducted under 10 mA cm^{-2} for 10h, with 1M KOH as the electrolyte, NiS_2 ($NiSe_2$, or Ni_5P_4) as the working electrode, Pt as the counter electrode, and Hg/HgO electrode as the reference electrode. The final product was denoted as X-NiOOH (X=NiS$_2$, NiSe$_2$, Ni$_5$P$_4$).

(4) Collection of X-Ni(OH)$_2$ (X=NiS$_2$, NiSe$_2$, Ni$_5$P$_4$) powder. The X-NiOOH (X=NiS$_2$, NiSe$_2$, Ni$_5$P$_4$) samples were washed in DI water for several times to remove the residual impurity species. Then, the samples were immersed into the absolute ethanol solution for 1h to fully transfer the NiOOH to $Ni(OH)_2$. Next, the X-Ni(OH)$_2$ (X=NiS$_2$, NiSe$_2$, Ni$_5$P$_4$) powder in absolute ethanol solution was obtained through a sonication process. After standing still for 1h, the upper solution was separated and dried at 70 °C for 24h. After that, the X-Ni(OH)$_2$ (X=NiS$_2$, NiSe$_2$, Ni$_5$P$_4$) powder was collected.

(5) Preparation of NiFe LDH. The NiFe LDH was grown on the carbon cloth via the same hydrothermal process as the synthesis of $Ni(OH)_2$.

Removal of Fe impurity. The 1M KOH solution was purified to remove Fe impurity before use. The procedure was as follows: First, 0.5 g $Ni(NO)_3 \cdot 6H_2O$ powder was added into 30 mL 1M KOH solution, forming $Ni(OH)_2$ precipitation. Next, the suspension was centrifuged at 10000 r/min for 3 times. The centrifugation process was repeated for 3 times. Then, the obtained $Ni(OH)_2$ powder was added into 50 mL KOH solution and mechanically agitated for 10 min. After standing still for

24h, the suspension was centrifuged with the KOH supernatant decanted into a clean electrochemical cell for use.

Material Characterizations. The XRD patterns were measured by a Bruker D8 X-ray diffractometer where the Cu Kα radiation (λ =1.5406Å) was equipped. The SEM images were obtained using ZEISS SEM Supra 40. The Raman spectra were recorded by a Raman Spectrophotometer with an excitation wavelength of 514.4 nm. The XPS was measured by a Kratos Analytical Axis Ultra DLD UHV spectrometer equipped with Al Kα X-ray irradiation source (1486.6 eV). Nickel K-edge X-ray absorption fine structure (XAFS) spectra were recorded at the XAFCA beamline at the Singapore Synchrotron Light Source(SSLS) under transmission mode where the storage ring is running at 0.7 GeV with current nearly 200mA.[1] The energy calibrations were finished by using standard Nickel foil. The k^2-weighted Fourier transforms were conducted using the Hanning window function for the EXAFS results, with the k-range of 2.5-10.5Å^{-1}. The Nickel $L_{2,3}$-edge and Oxygen K-edge Near-edge X-ray absorption fine structure (NEXAFS) spectra were also recorded at the SUV beamline of SSLS. The data was collected under total electron yield mode with the photon energy resolution of 350 meV. The photon energy was calibrated through the characteristic intensity dip based on the contamination carbon of the beamline optical components at 284.4 eV. The NEXAFS data was normalized to the incident photon intensity (I_0) monitored by the focusing mirror. The particle size analysis was conducted via Zetasizer.

Electrochemical measurements.

All the electrochemical measurements were performed using an electrochemical workstation (VPM3, BiO-logic Inc) in a three-electrode setup in 1M KOH. The workstation is equipped with built-in electrochemical impedance spectroscopy (EIS) analyser. The working electrode was the X-NiOOH (X=NiS$_2$, NiSe$_2$, Ni$_5$P$_4$). The Hg/HgO was chosen as the reference electrode. The Pt was used as the counter electrode. The linear scan voltammetry (LSV) was measured at scan rate 0.1 mV s^{-1}. The Tafel plots were derived by plotting the overpotential η(mV) versus the log current density(log[J]). The Tafel slope was obtained via linearly fitting the linear portion of the Tafel plots according to the Tafel equation (η =b log[J] +a, b is the Tafel slope). The potential electrochemical impedance spectroscopy (EIS) measurements were conducted at open circuit potential with the frequency set from 10 mHz to 100 kHz.

Electrochemically surface area. The electrochemically surface area (ECSA) data was evaluated from recording the electrochemical double-layer capacitance of the catalyst via cyclic voltammograms (CVs). Here, the potential range was set at 0.02-0.12 V (versus Hg/HgO) to avoid the Faradaic process. The CVs were conducted in the quiescent electrolyte with the potential swept across the set potential range with at 6 scan rates 5, 10, 20, 30, 40, 50 mV s^{-1}. The charging current was plotted versus scan rate and a straight line could be derived with the slope value equalled to the double-layer capacitance (C_{dl}). The ECSA was obtained by dividing the C_{dl} to the specific capacitance C_s = 0.04 mF cm^{-2}.[2]

Pulse-voltammetry test.[3] For preparing glassy carbon electrode, 4 mg of the collected X-Ni(OH)$_2$(X=NiS$_2$, NiSe$_2$, Ni$_5$P$_4$) powder was added into the 750 uL DI water, 250 uL isopropanol and 20 uL (5wt.%) Nafion solution followed by at least 60 min sonication to obtain a uniform ink. Then 10 uL of the ink was pipetted onto the glassy carbon (loading mass:0.516 mg cm^{-2}) and air dried at room-temperature for 12 h before electrochemical tests. Before the pulse voltammetry (P-V) test, an electrochemical activation process under 10 mA cm^{-2} for 1h in 1M KOH electrolyte was applied for the samples coated on the glassy carbon electrode. The potential was set firstly at a low potential (E_l) for 6s, then turned to a higher potential (E_h) for 6s before back to E_l for 6s.

This cycle was repeated while increasing E_h from 1.42 V to 1.68 V versus RHE in 20 mV/step with constant $E_l = 1.4$ V. The transferred charge normalized to ECSA during each cycle was evaluated by integrating the current pulse/ECSA over time.

Computational method. All calculations were conducted via the DFT with the generalized Perdew-Burke-Ernzerhof (PBE), and the projector augmented-wave (PAW) pseudopotential planewave method as implemented in the Vienna *ab initio* Simulation Package (VASP) code. The X-Ni(OH)$_2$ (X=NiS$_2$, NiSe$_2$, Ni$_5$P$_4$) and benchmark Ni(OH)$_2$ construction are based on the fitted Ni-O bond distances results. (Table. S2)
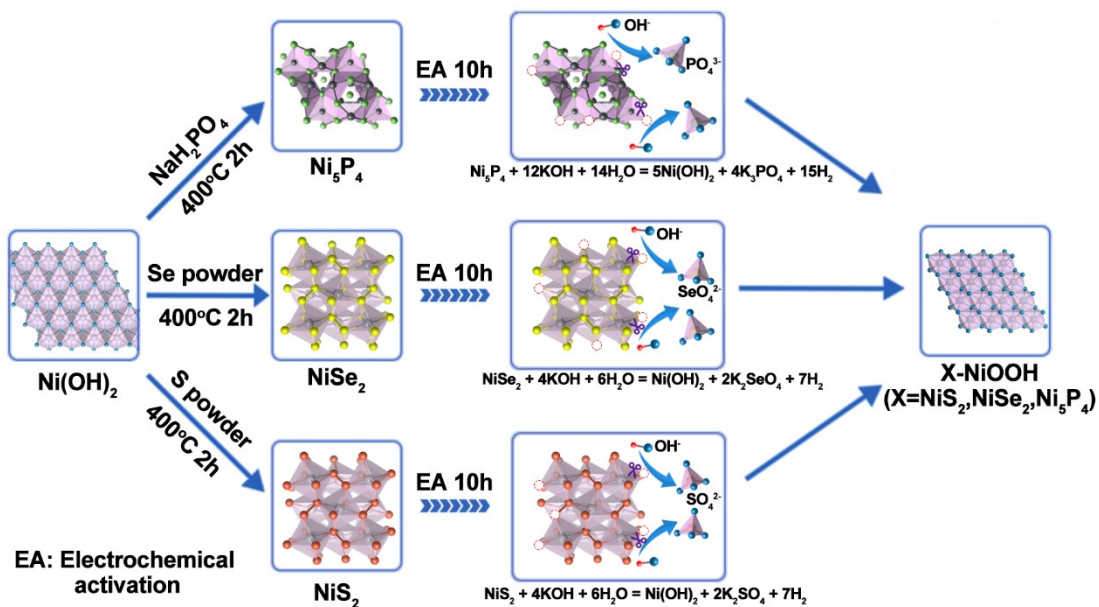
Fig. S1.

Schematic illustration of the synthesis route for the $NiS_2/NiSe_2/Ni_5P_4$-NiOOH. All the experimental procedures are kept the same except for the anion source.
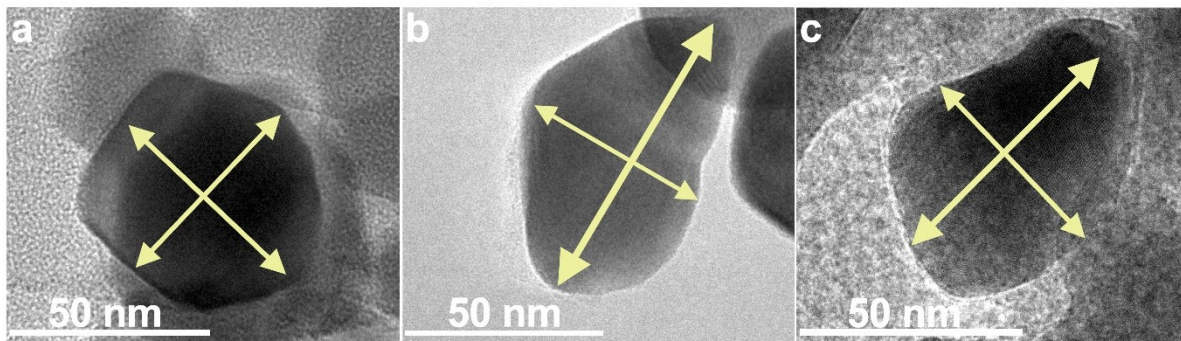
Fig. S2.

(a) TEM image of NiS_2, the estimated area of the highlighted particle was ~ 2931 nm^2. (b) TEM image of $NiSe_2$, the estimated area of the highlighted particle was ~3011 nm^2. (c) TEM image of Ni_5P_4, the estimated area of the highlighted particle was ~2734 nm^2.
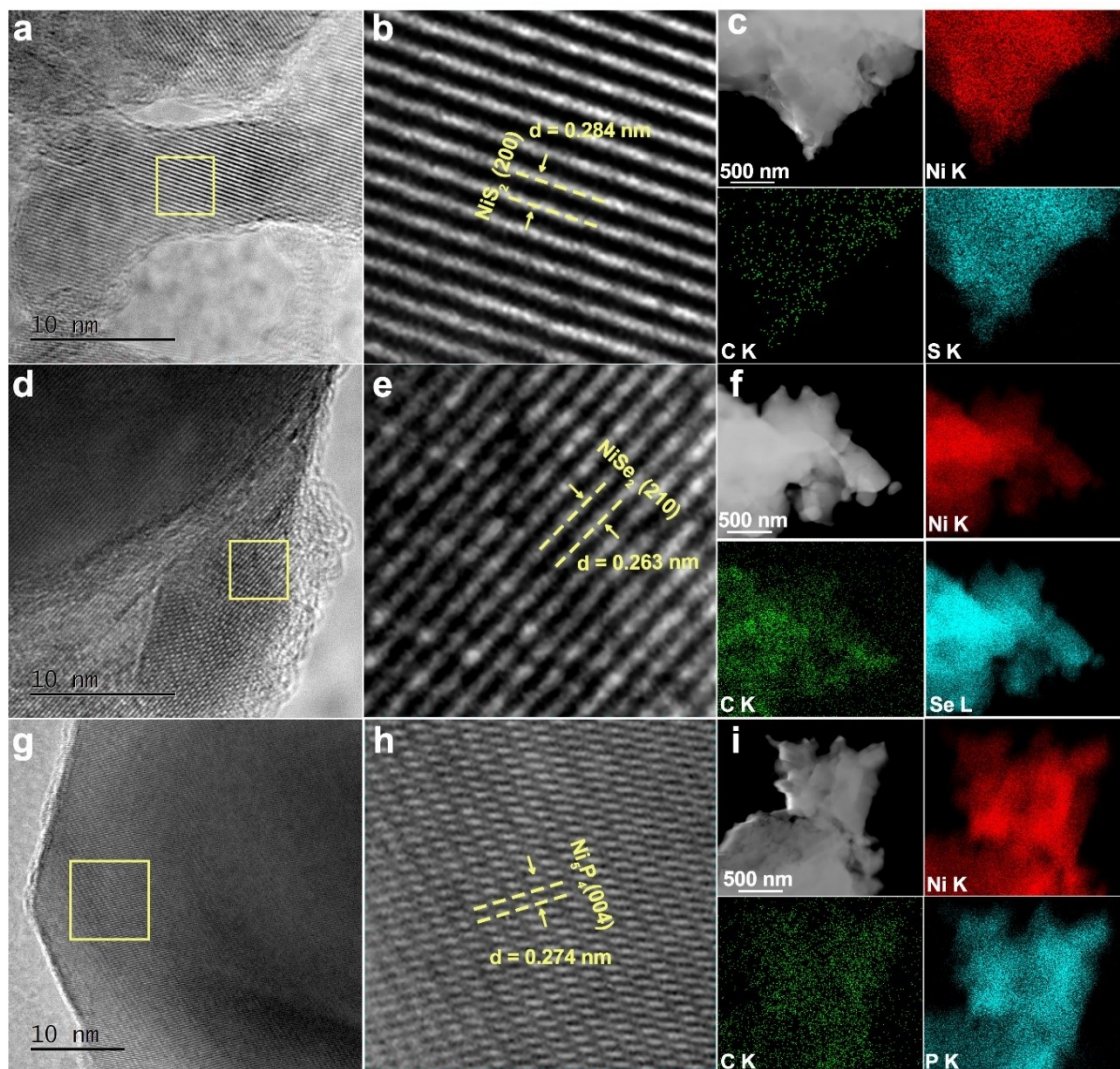
Fig. S3.

(a) HRTEM image of NiS$_2$. (b) magnified region as indicated by the rectangular area in (a). (c) TEM image and corresponding EDS elemental mapping of NiS$_2$. (d) HRTEM image of NiSe$_2$. (e) magnified region as indicated by the rectangular area in (d). (f) TEM image and corresponding EDS elemental mapping of NiSe$_2$. (g) HRTEM image of Ni$_5$P$_4$. (h) magnified region as indicated by the rectangular area in (g). (i) TEM image and corresponding EDS elemental mapping of NiSe$_2$.
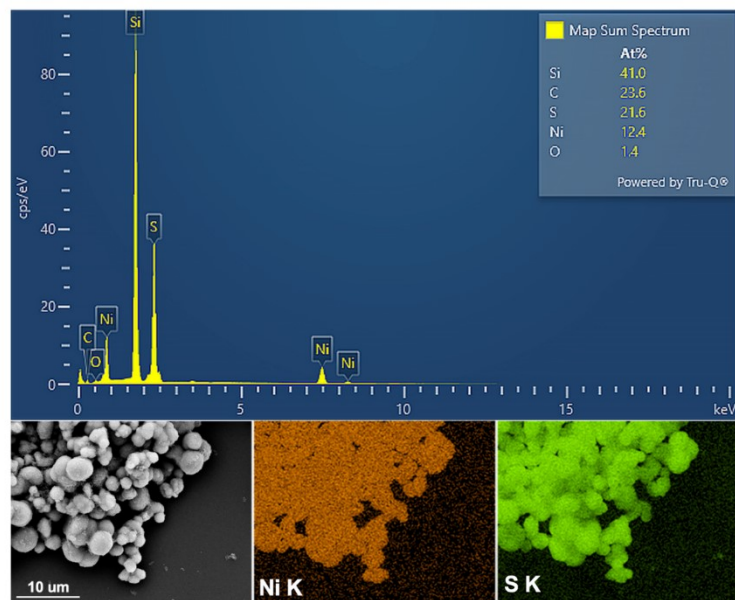
Fig. S4.

SEM-EDS result of NiS_2 pre-catalyst. Uniform distributions of Ni and S were recorded.
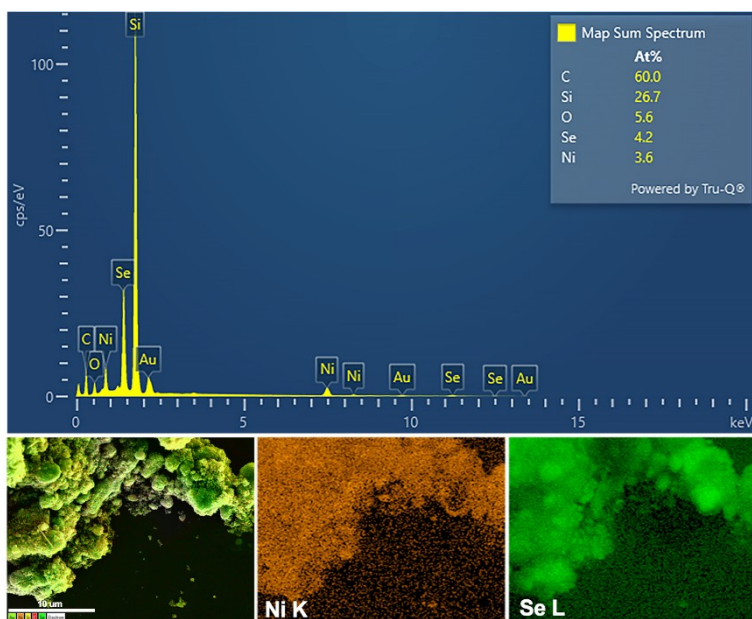
Fig. S5.

SEM-EDS result of NiSe$_2$ pre-catalyst. Uniform distributions of Ni and Se were recorded.
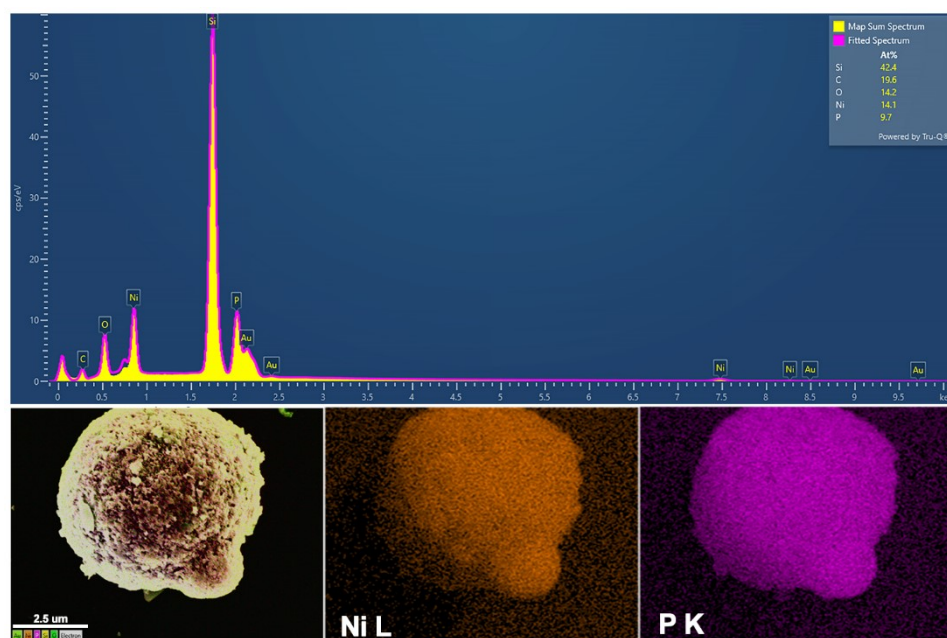
Fig. S6.
SEM-EDS result of Ni_5P_4 pre-catalyst. Uniform distributions of Ni and P were recorded.
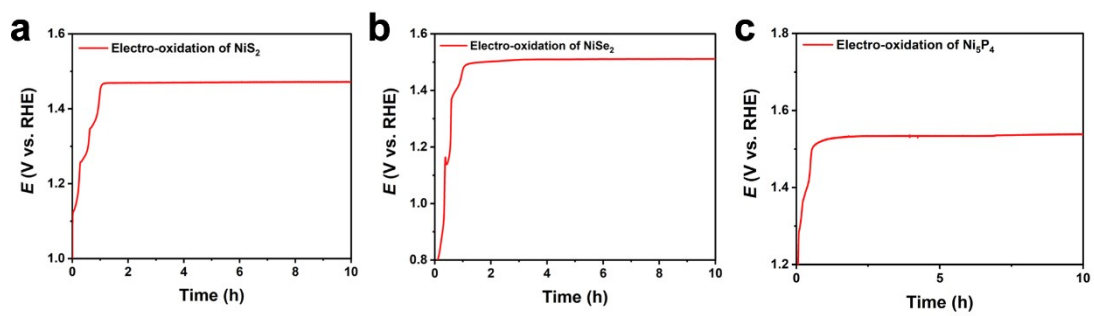
Fig. S7.

The electro-oxidation of prepared (a)NiS_2, (b) $NiSe_2$, (c) Ni_5P_4 using Chronopotentiometry. The electro-oxidation current density is set as 10 mA cm^{-2}.
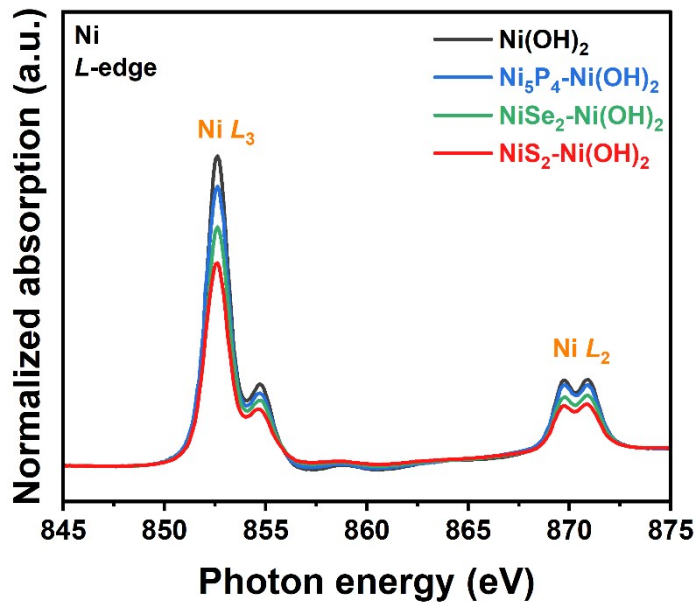
Fig. S8. Ni $L_{2,3}$-edge spectra of X-Ni(OH)$_2$ (X=NiS$_2$,NiSe$_2$,Ni$_5$P$_4$) with Ni(OH)$_2$ as benchmark.

These X-Ni(OH)$_2$ all show quite similar profile in comparison with Ni(OH)$_2$, indicating roughly all of the Ni atoms are arranged in the NiO$_6$ octahedral site.
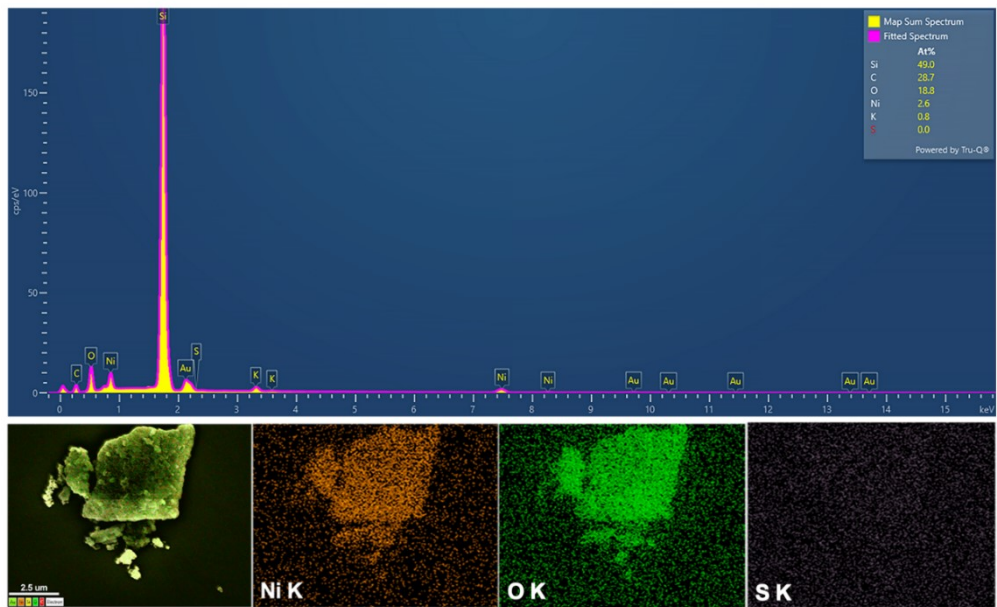
Fig. S9.

SEM-EDS result of NiS2-Ni(OH)$_2$.No S signal was detected.
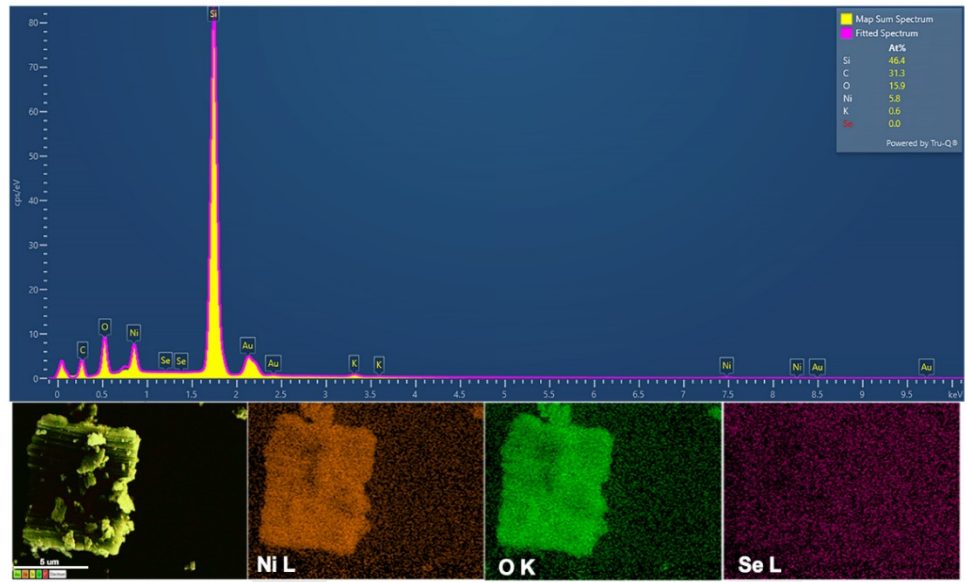
Fig. S10.

SEM-EDS result of NiSe$_2$-Ni(OH)$_2$. No Se signal was detected.
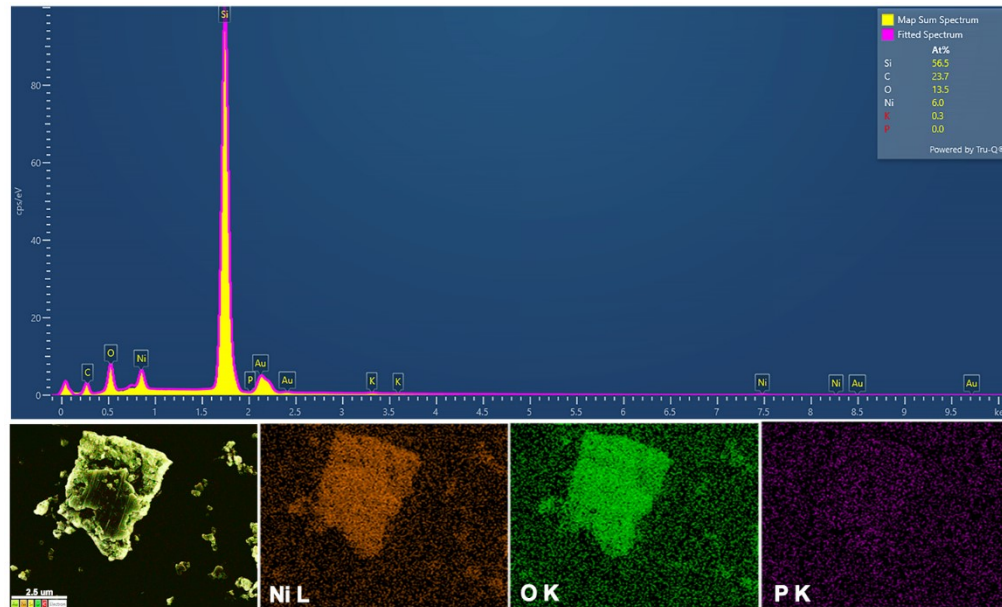
Fig. S11.
SEM-EDS result of Ni$_5$P$_4$-Ni(OH)$_2$. No P signal was detected.
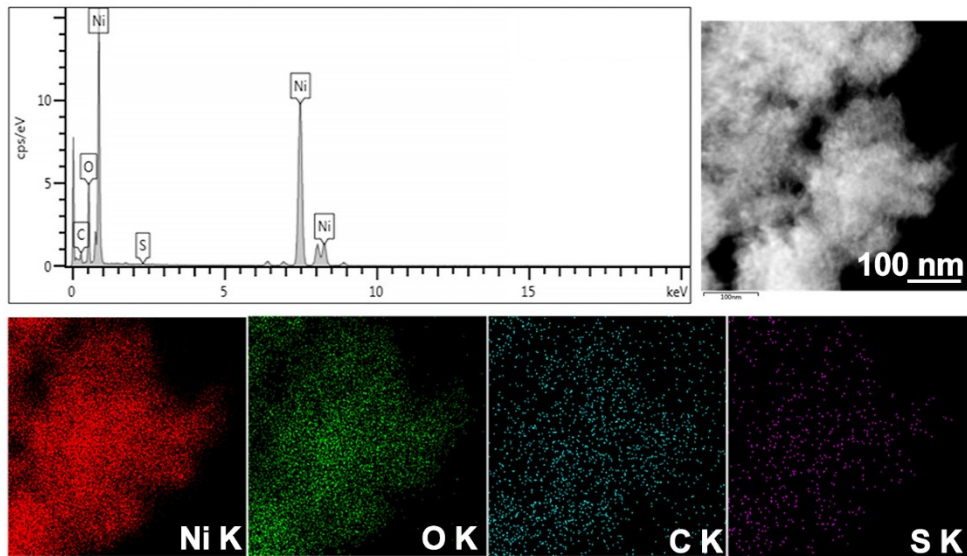
Fig. S12.

TEM-EDS result of NiS_2-$Ni(OH)_2$. The atomic Ni, O, C, and S compositions were 70.61%, 24.35%, 4.92%, and 0.12%, respectively.
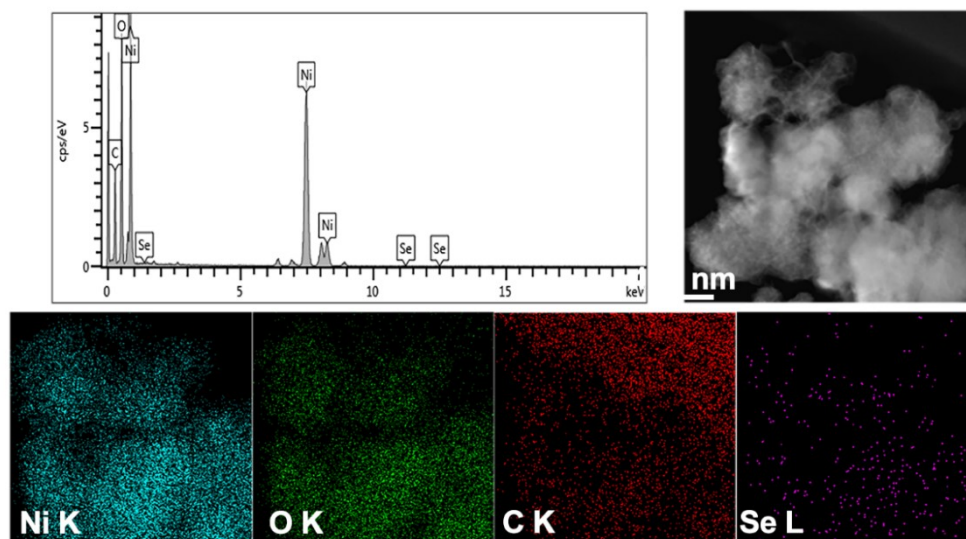
Fig. S13.

TEM-EDS result of NiSe$_2$-Ni(OH)$_2$. The atomic Ni, O, C, and Se compositions in the material were 40.35%, 36.62%, 23.03%, and 0.00%, respectively.
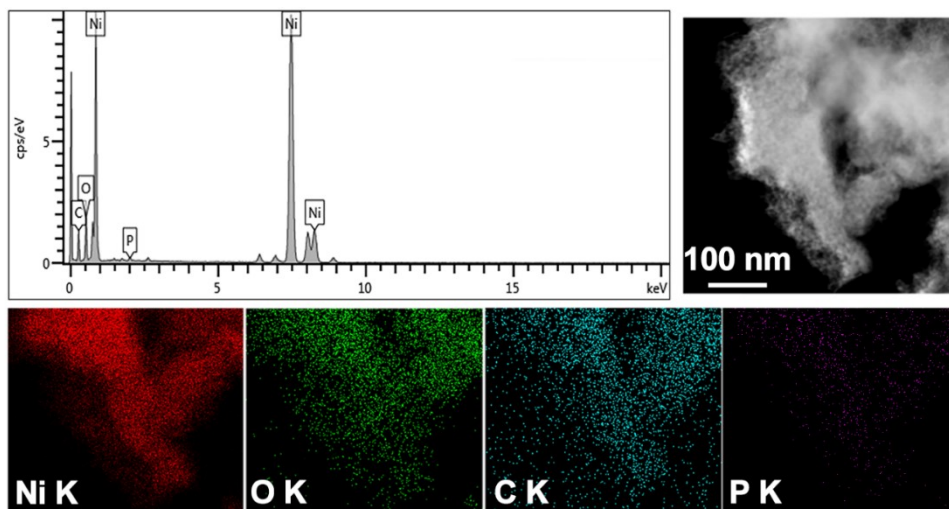
Fig. S14.

TEM-EDS result of Ni_5P_4-$Ni(OH)_2$. The atomic Ni, O, C, and P compositions in the material were 78.91%, 9.84%, 10.94%, and 0.31%, respectively.
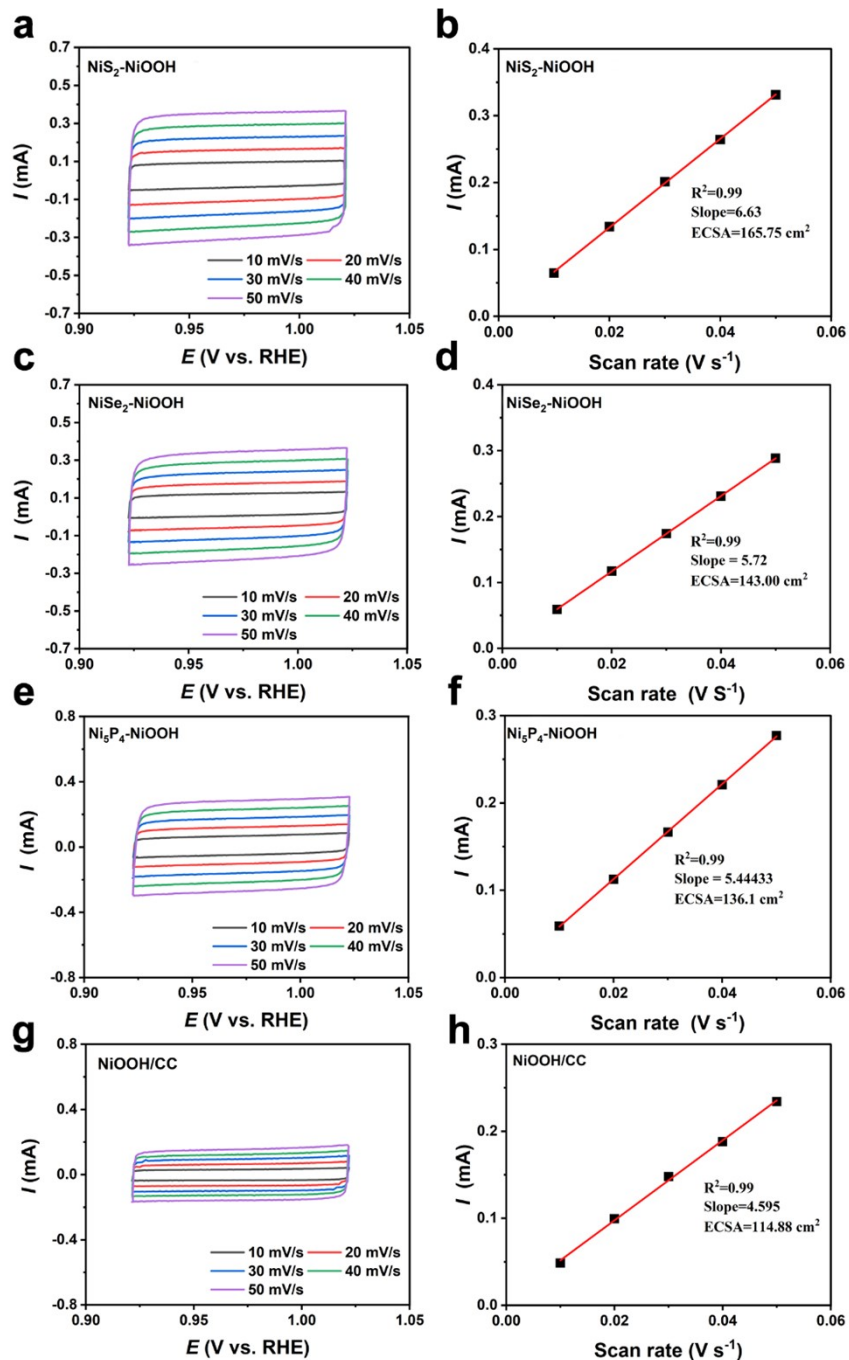
Fig. S15.

The Cyclic voltammograms curves and current vs. scan rate plots of the (a)-(b) NiS_2-NiOOH (c)-(d) $NiSe_2$-NiOOH, (e)-(f) Ni_5P_4-NiOOH, (g)-(h) NiOOH. Plots of current vs. scan rate data were obtained from CV curves at 0.98 V. The ECSA for all samples was calculated as: NiS_2-NiOOH (165.75 cm^2), $NiSe_2$-NiOOH (143.00 cm^2), Ni_5P_4-NiOOH (136.10 cm^2), and NiOOH (114.88 cm^2).
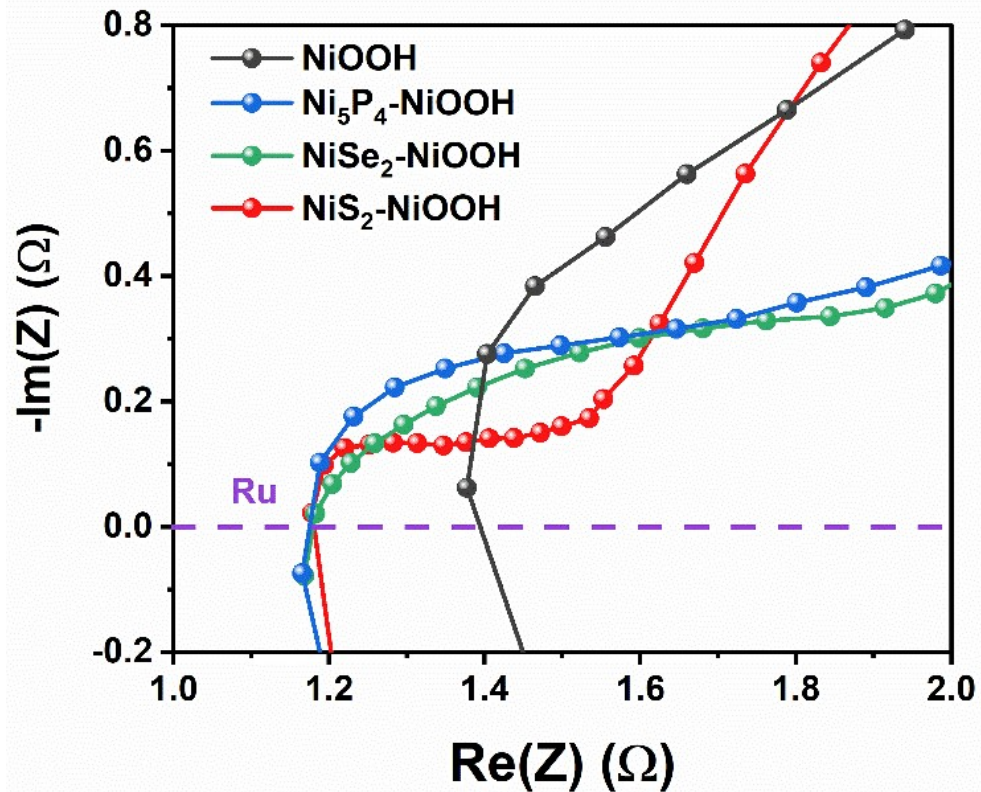
Fig. S16.

Potential electrochemical impedance spectroscopy data for X-NiOOH (X=NiS$_2$, NiSe$_2$, Ni$_5$P$_4$) and benchmark NiOOH obtained at open circuit potential. The Ru (solution resistance) is used for *iR*-correction, which is 1.18 Ω, 1.18 Ω, 1.17 Ω, 1.40 Ω for NiS$_2$-NiOOH, NiSe$_2$-NiOOH, Ni$_5$P$_4$-NiOOH, and NiOOH, respectively.
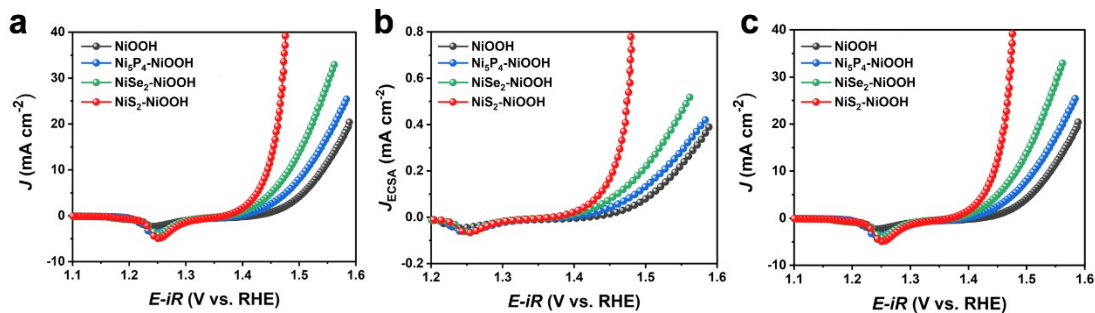
Fig. S17.

(a) OER polarization curves of the X-NiOOH (X = NiS_2, $NiSe_2$, Ni_5P_4) after *iR*-correction. (b) OER polarization curves of the X-NiOOH (X = NiS_2, $NiSe_2$, Ni_5P_4) after *iR*-correction normalization to ECSA. (c) OER polarization curves of the X-NiOOH (X = NiS_2, $NiSe_2$, Ni_5P_4) after *iR*-correction normalization to mass loading, which are 1.06 mg/cm^2, 1.10 mg/cm^2, 0.97 mg/cm^2, and 0.95 mg/cm^2 for NiS_2-NiOOH, $NiSe_2$-NiOOH, Ni_5P_4-NiOOH, and NiOOH.
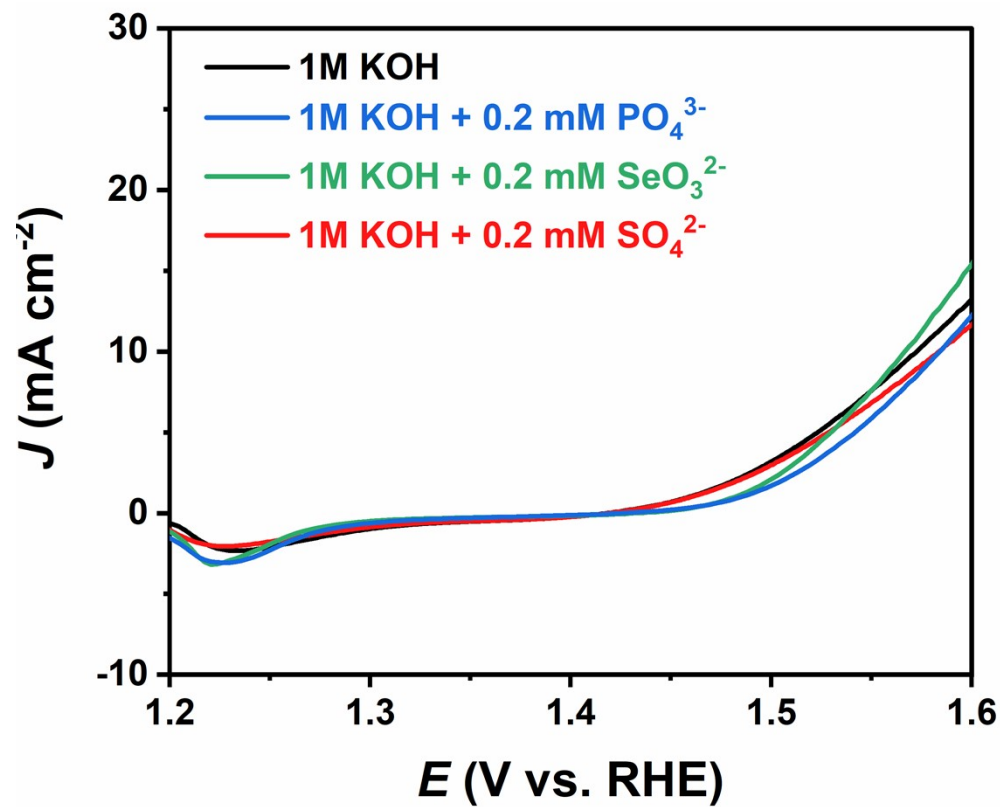
Fig. S18.
The influence of dissolute anion species on the OER activity of NiOOH. The overpotentials are 343 mV, 355 mV, 337 mV, 353 mV for NiOOH in 1M KOH, 0.2 mM PO_4^{3-} + 1M KOH, 0.2 mM SeO_3^{2-} + 1M KOH, 0.2 mM SO_4^{2-} + 1M KOH solution, respectively.
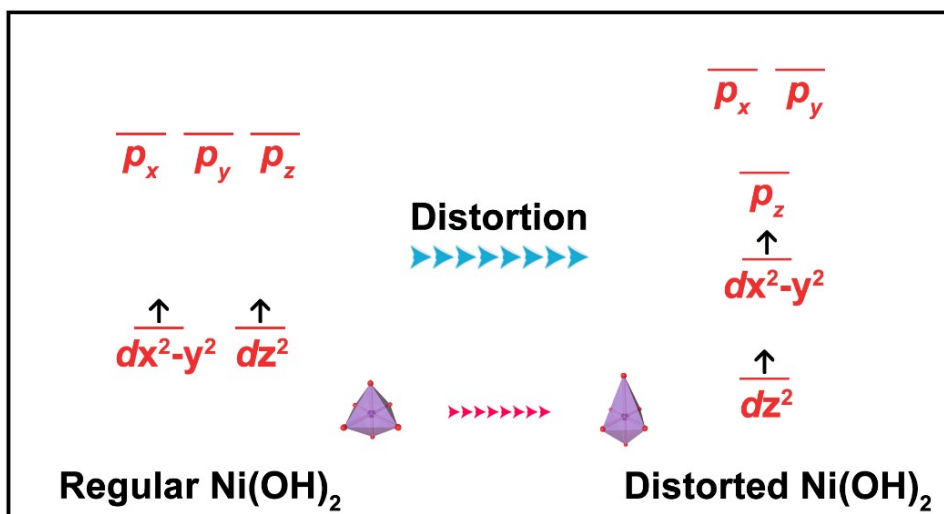
Fig. S19.

The orbital diagram of regular high spin Ni^{2+}. The NiO_6 octahedron distortion would lead to the $4p$ orbital and e_g^* orbital splitting.
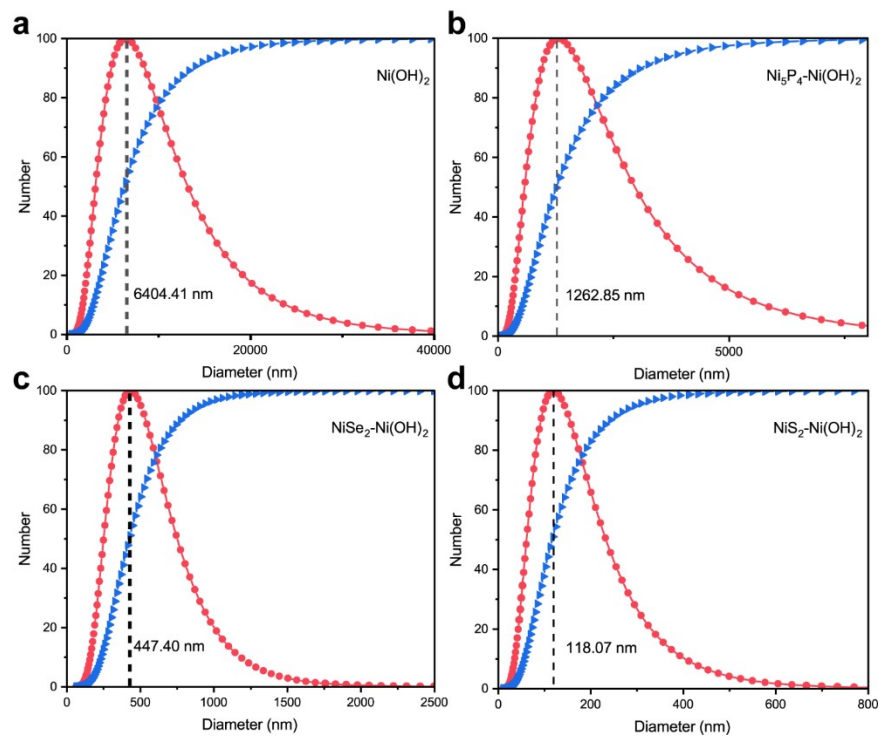
Fig. S20.

Particle size distribution analysis by Zetasizer for X-Ni(OH)$_2$ (X=S, Se, P) and hydrothermal prepared Ni(OH)$_2$.
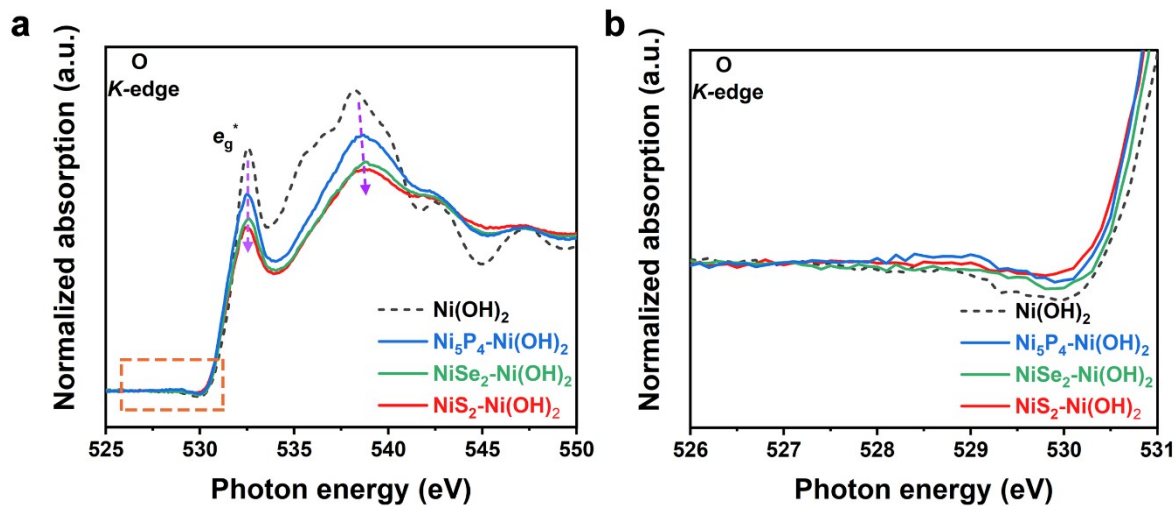
Fig. S21.

a. Normalized O *K*-edge XAS spectra of X-Ni(OH)$_2$ (X=NiS$_2$, NiSe$_2$, Ni$_5$P$_4$) with hydrothermal prepared Ni(OH)$_2$ as benchmark. **b.** Enlarged O *K* pre-edge region from **a**.
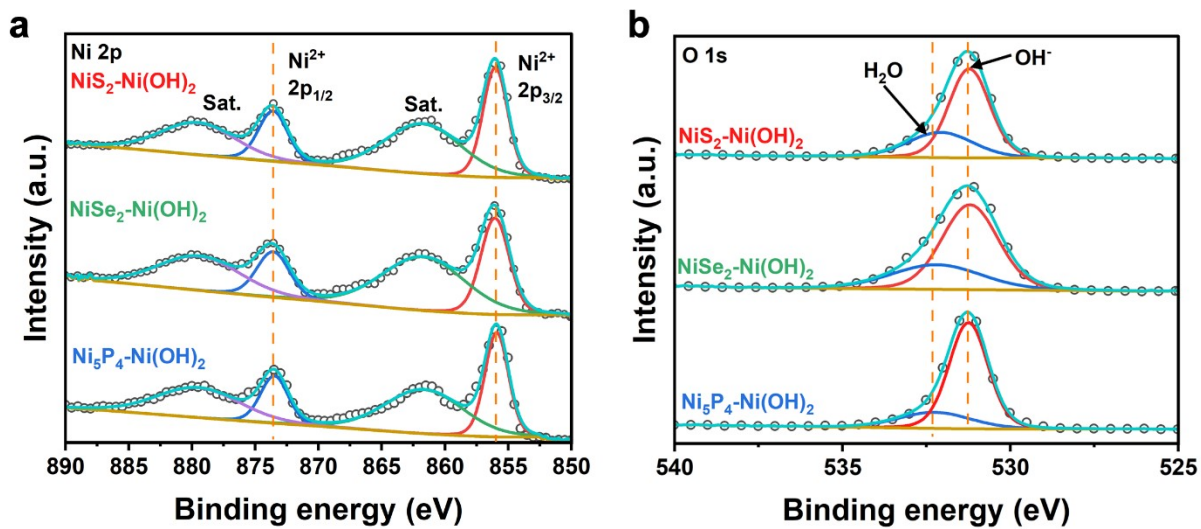
Fig. S22.

a. Ni 2p XPS spectra of X-Ni(OH)$_2$ (X= NiS$_2$, NiSe$_2$, Ni$_5$P$_4$). **b.** O 1s XPS spectra of X-Ni(OH)$_2$ (X= NiS$_2$, NiSe$_2$, Ni$_5$P$_4$).
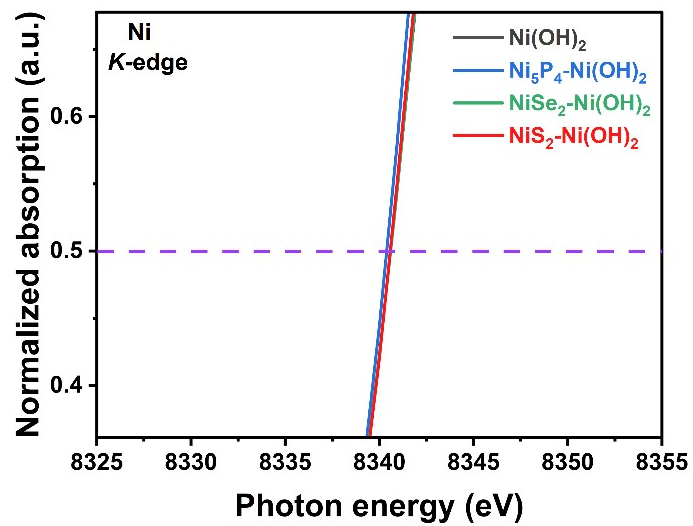
Fig. S23.

Magnified absorption ~0.5 region of Ni *K*-edge spectra.
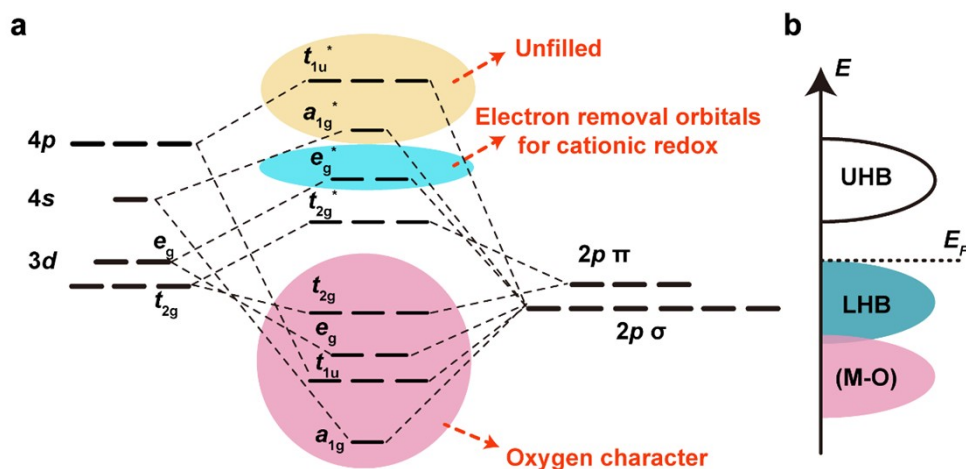
Fig. S24.

(a) The molecular orbital diagram of octahedral NiO_6. (b)Schematic energy band of NiO_6 in consideration of Mott-Hubbard splitting. For the bonding bands including a_{1g}, t_{1u}, e_g, and t_{2g}, they show oxygen character (denoted as M-O). For the antibonding bands $(M\text{-}O)^*$, *i.e.*, t_{2g}^*, a_{1g}^*, t_{1u}^*, and e_g^*, they show metal character. Here, t_{2g}^* contains d_{xy}, d_{yz} and d_{xz} orbitals and e_g^* includes d_{z^2} and $d_{x^2-y^2}$ orbitals, respectively. Among these electronic bands, the (M-O) and t_{2g}^* are fully occupied, while e_g^* is partially occupied with one spin-up electron each in the d_{z^2} orbital and $d_{x^2-y^2}$ orbital. Due to the on-site electron repulsion within the d orbitals, antibonding bands will split into an empty upper- and filled lower-Hubbard bands (denoted as UHB and LHB, respectively), with an energy difference U.
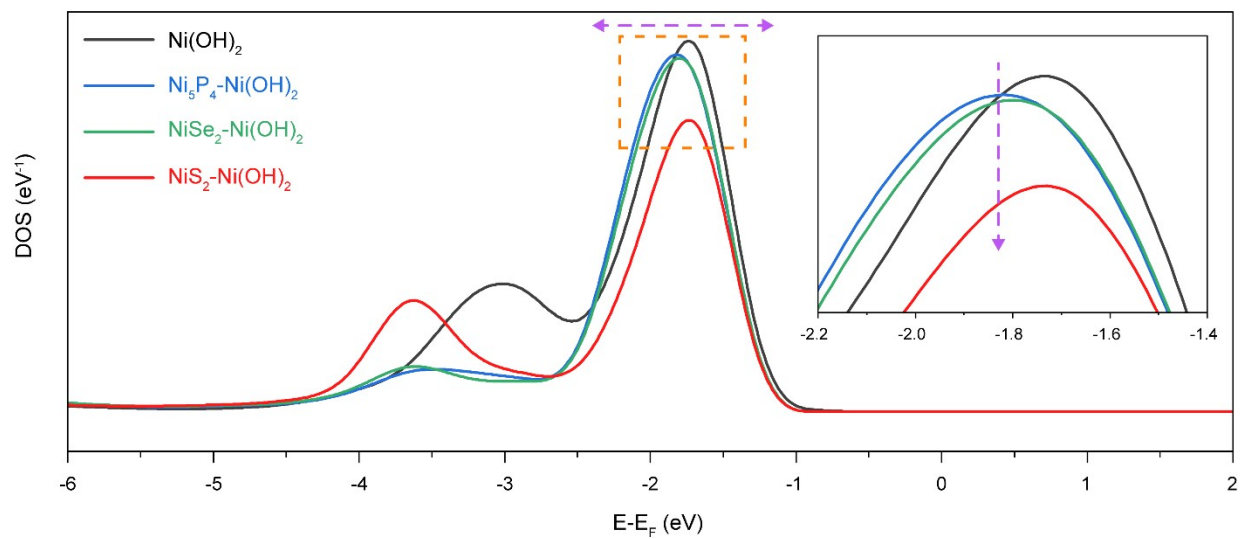
Fig. S25.
The calculated e_g^* band density of states (DOS) of X-Ni(OH)$_2$ (X = NiS$_2$, NiSe$_2$ and Ni$_5$P$_4$).
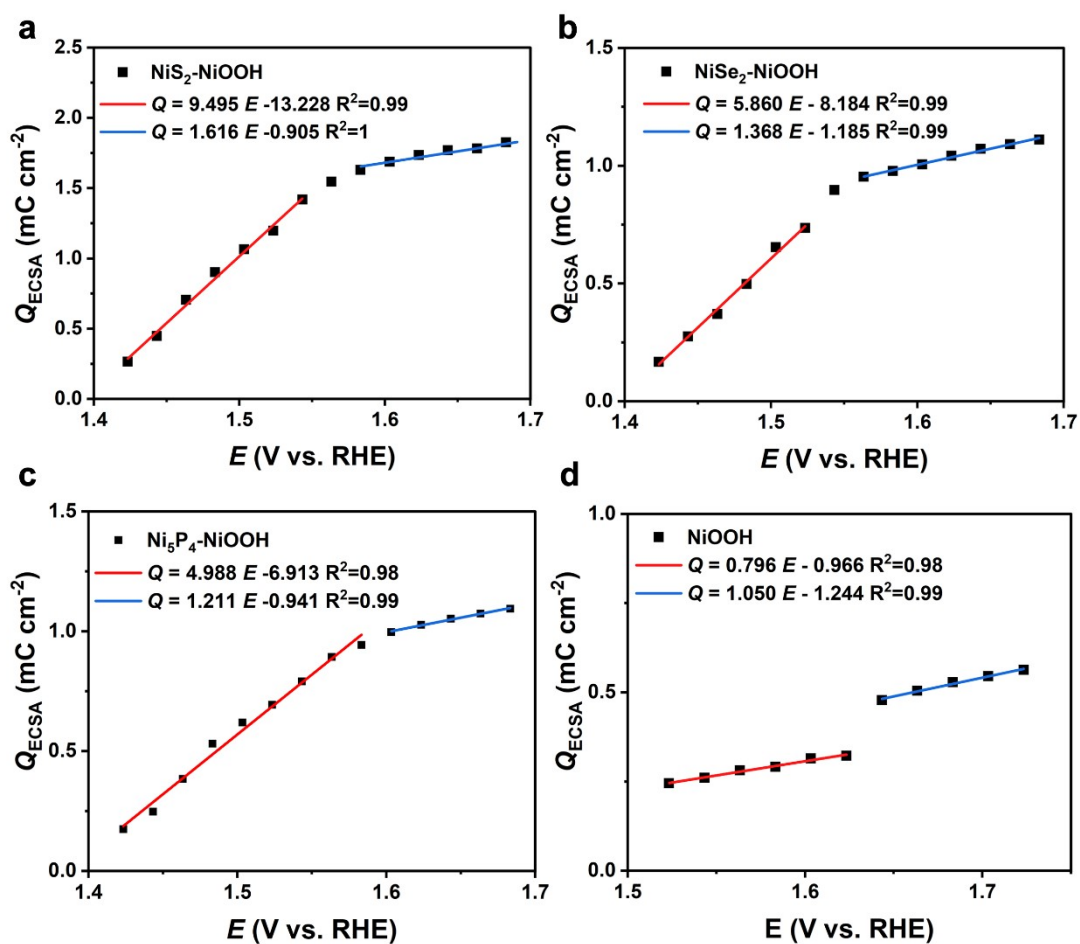
Fig. S26.

Potential versus log(current) from pulse voltammetry. (normalization to ECSA) (a) NiS_2-NiOOH. (b) $NiSe_2$-NiOOH. (c) Ni_5P_4-NiOOH. (d) NiOOH. The slope is used to represent the charge transfer ability.
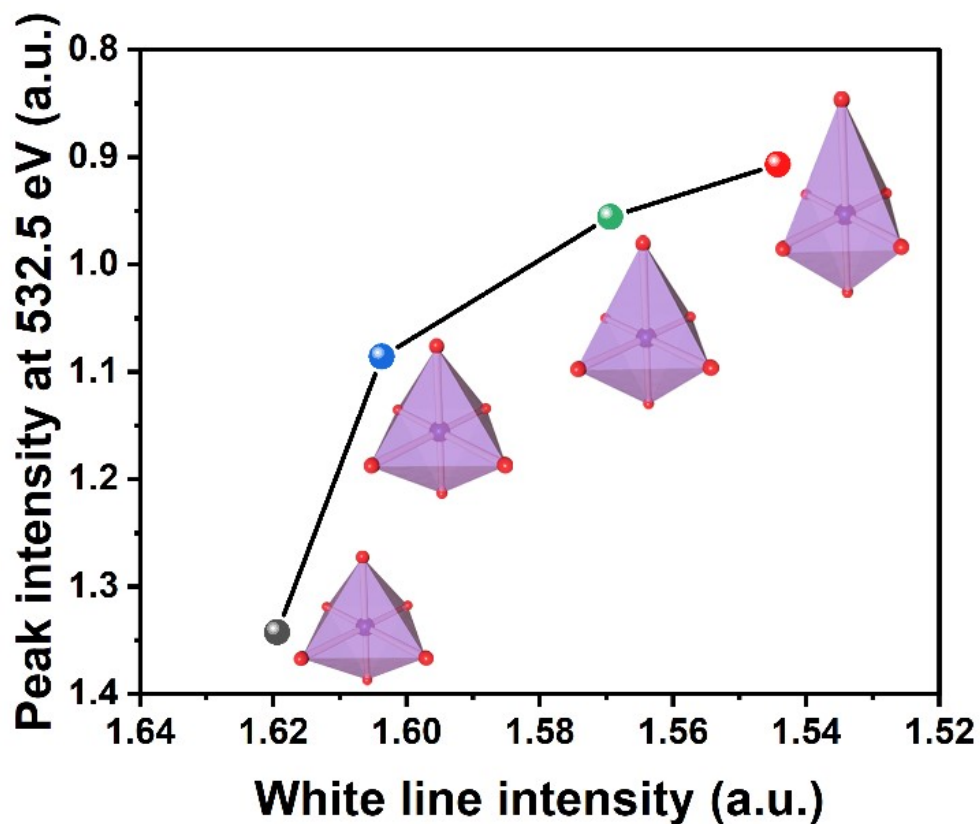
Fig. S27.

The correlation between NiO_6 distortion and e_g^* band broadening. Here, the normalized white line intensity from Ni *K*-edge spectra (Fig. 3a) is used to identify the geometry distortion extent in $Ni(OH)_2$. On the other hand, the normalized peak intensity at 532.5 eV adopted from Fig.3d (corresponding to the e_g^* splitting) is used to represent the e_g^* band broadening extent around the Fermi level.
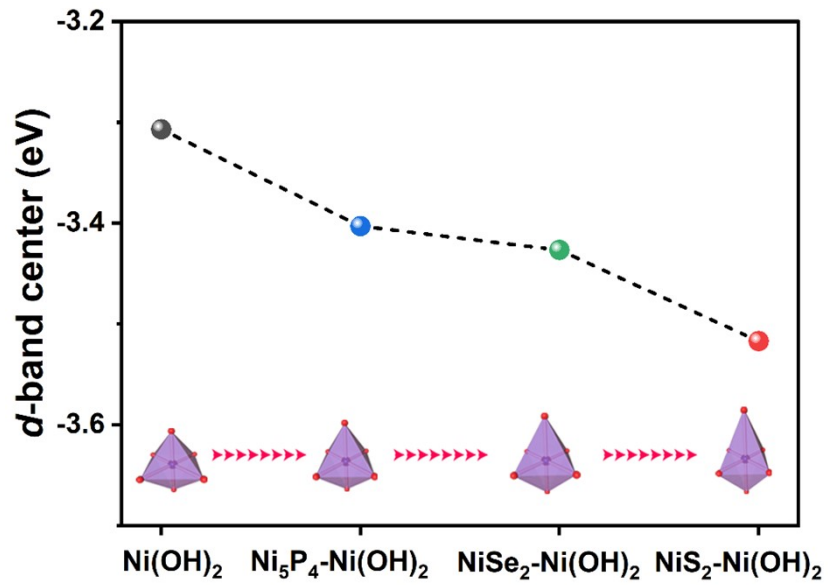
Fig. S28.

Calculated d-band center for X-Ni(OH)$_2$ (X=NiS$_2$, NiSe$_2$, Ni$_5$P$_4$)
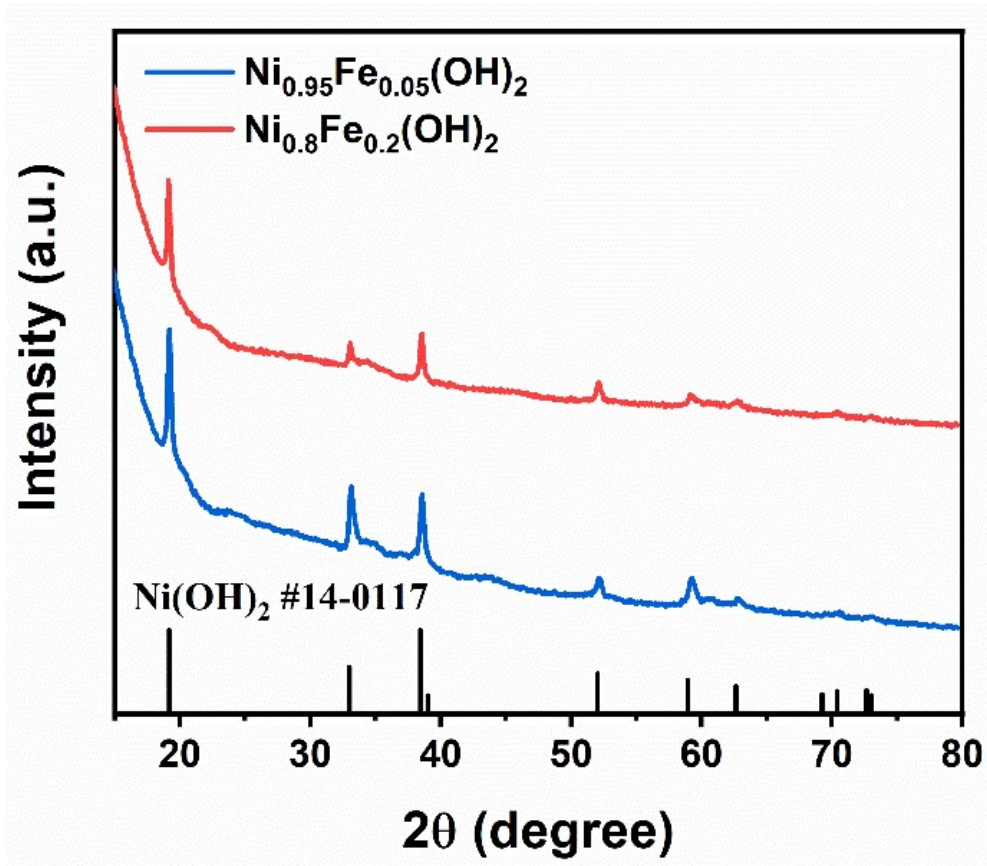
Fig. S29.
The XRD results of $Ni_{0.95}Fe_{0.05}(OH)_2$ and $Ni_{0.8}Fe_{0.2}(OH)_2$.
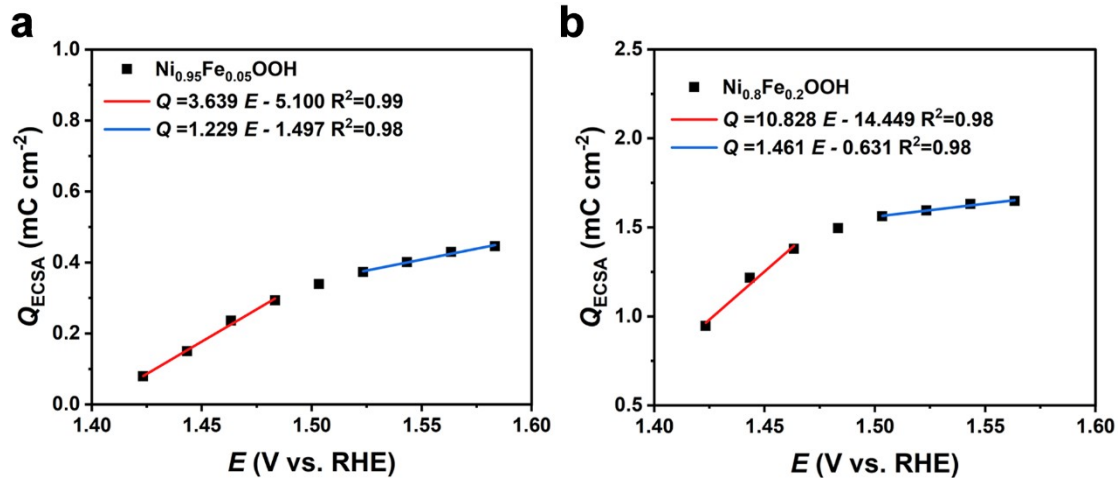
Fig. S30.

Potential versus log(current) from pulse voltammetry. (normalized to ECSA) (a) $Ni_{0.95}Fe_{0.05}OOH$. (b) $Ni_{0.8}Fe_{0.2}OOH$.
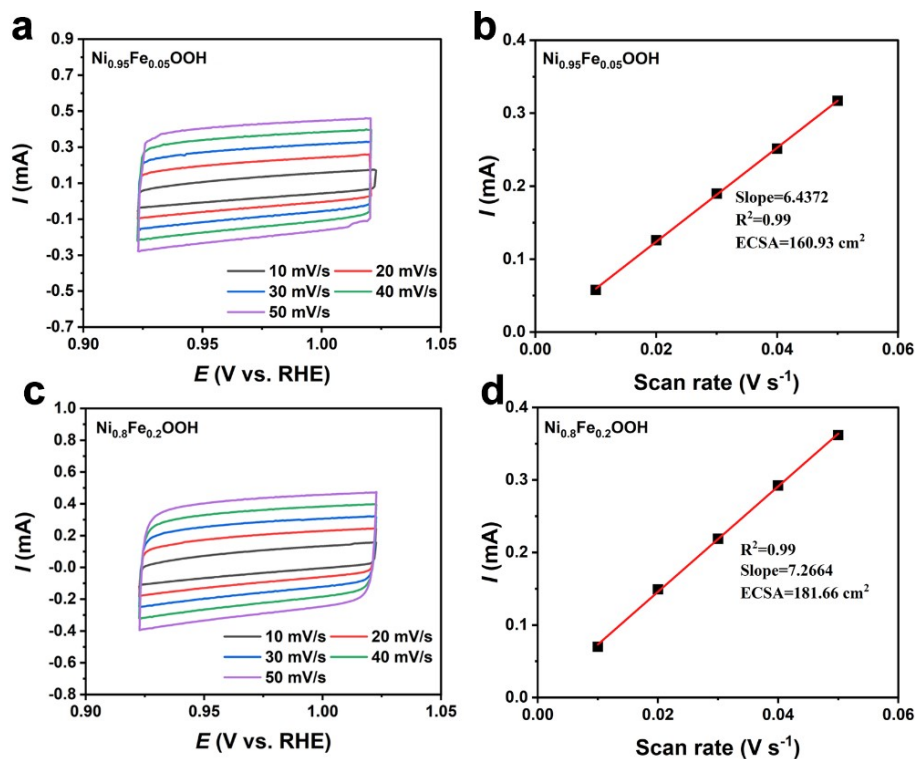
Fig. S31.

The Cyclic voltammograms curves and current vs. scan rate plots of the (a)-(b) $Ni_{0.95}Fe_{0.05}OOH$, (c)-(d) $Ni_{0.8}Fe_{0.2}OOH$. Plots of current vs. scan rate data were obtained from CV curves at 0.98 V. The ECSA for all samples was calculated as: $Ni_{0.95}Fe_{0.05}OOH/CC$ (160.93 cm^2), $Ni_{0.8}Fe_{0.2}OOH/CC$ (181.66 cm^2).
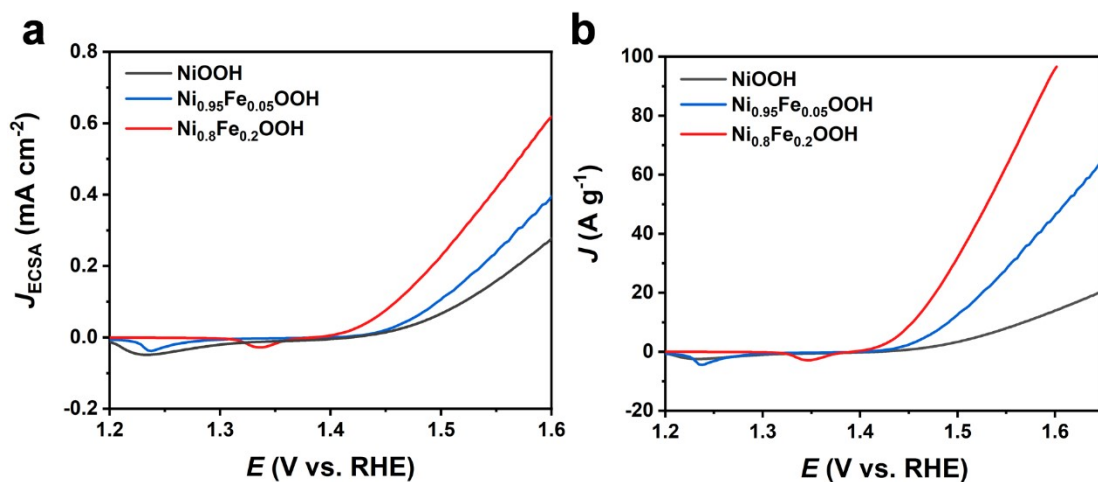
Fig. S32.

(a) OER polarization curves of the $Ni_xFe_{1-x}OOH$ (x=1, 0.95, 0.8) normalization to ECSA. (b) OER polarization curves of the $Ni_xFe_{1-x}OOH$ (x=1, 0.95, 0.8) normalization to mass loading. The NiOOH is regards as the active species and its loading mass in $Ni_{0.95}Fe_{0.05}OOH$ and $Ni_{0.8}Fe_{0.2}OOH$ is evaluated as 0.55 mg cm^{-2}, and 0.51 mg cm^{-2}, respectively.
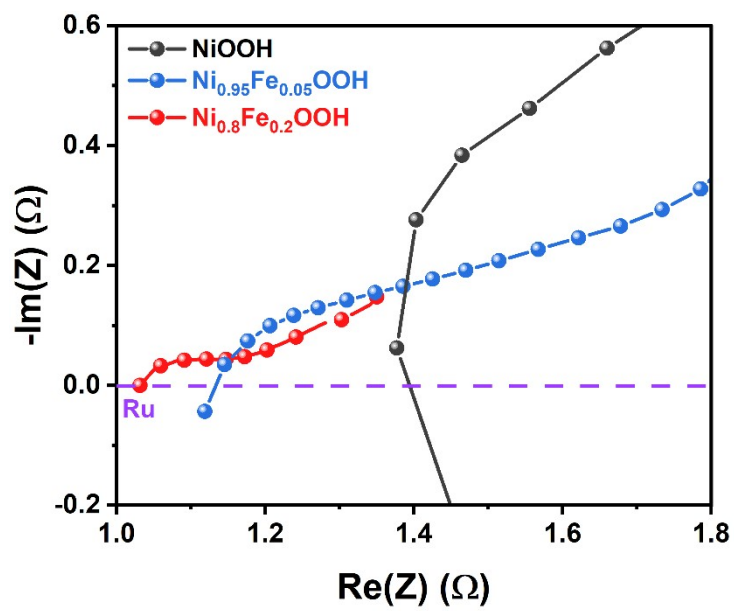
Fig. S33.
Potential electrochemical impedance spectroscopy data for $Ni_{1-x}Fe_xOOH$ (x=0, 0.05, 0.2) at open circuit potential. Ru (solution resistance) was used for *IR*-correction, which was 1.03 Ω, 1.13 Ω, 1.40 Ω for $Ni_{0.8}Fe_{0.2}OOH$, $Ni_{0.95}Fe_{0.05}OOH$, and NiOOH, respectively.
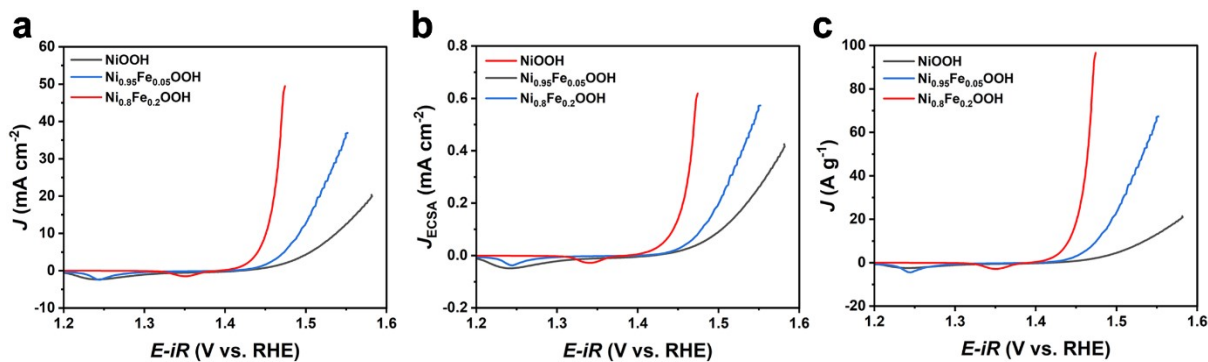
Fig. S34.

(a) OER polarization curves of $Ni_{1-x}Fe_xOOH$ (x=0, 0.05, 0.2) after iR-correction. (b) OER polarization curves of $Ni_{1-x}Fe_xOOH$ (x=0, 0.05, 0.2) after iR-correction normalized to ECSA. (c) OER polarization curves of $Ni_{1-x}Fe_xOOH$ (x=0, 0.05, 0.2) after iR-correction normalized to mass loading. NiOOH is regarded as the active species and its loading mass in $Ni_{0.95}Fe_{0.05}OOH$ and $Ni_{0.8}Fe_{0.2}OOH$ was evaluated as 0.55 mg cm^{-2}, and 0.51 mg cm^{-2}, respectively.

Table S1.

ICP/CNHS results of NiS_2, $NiSe_2$, and Ni_5P_4 before and after chronopotentiometry treatment

Samples	Ni (w/w%)	S(w/w%)	Se(w/w%)	P(w/w%)
NiS_2	44.11	51.79	\	\
NiS_2-$Ni(OH)_2$	45.35	N/A	\	\
$NiSe_2$	23.46	\	66.51	\
$NiSe_2$-$Ni(OH)_2$	43.57	\	0.13	\
Ni_5P_4	65.85	\	\	28.26
Ni_5P_4-$Ni(OH)_2$	41.27	\	\	0.08

Table S2.

Fitted mean Ni-O bond distances in X-Ni(OH)$_2$ (X= NiS$_2$, NiSe$_2$, Ni$_5$P$_4$) and benchmark Ni(OH)$_2$

Samples	R(Å)
NiS$_2$-Ni(OH)$_2$	2.03916
NiSe$_2$-Ni(OH)$_2$	2.04688
Ni$_5$P$_4$-Ni(OH)$_2$	2.04875
Ni(OH)$_2$	2.05876

Reference list:

1. Y. Du, Y. Zhu, S. Xi, P. Yang, H. O. Moser, M. B. Breese and A. Borgna, *Journal of synchrotron radiation*, 2015, **22**, 839-843.
2. C. C. McCrory, S. Jung, J. C. Peters and T. F. Jaramillo, *J Am Chem Soc*, 2013, **135**, 16977-16987.
3. H. N. Nong, L. J. Falling, A. Bergmann, M. Klingenhof, H. P. Tran, C. Spori, R. Mom, J. Timoshenko, G. Zichittella, A. Knop-Gericke, S. Piccinin, J. Perez-Ramirez, B. R. Cuenya, R. Schlogl, P. Strasser, D. Teschner and T. E. Jones, *Nature*, 2020, **587**, 408-413.